Folding Thermodynamics and Kinetics of YNMG RNA Hairpins: Specific Incorporation of 8-Bromoguanosine Leads to Stabilization by Enhancement of the Folding Rate†

David J. Proctor,‡ Hairong Ma,§ Elzbieta Kierzek,|| Ryszard Kierzek,|| Martin Gruebele,*,§ and Philip C. Bevilacqua*,‡

Department of Chemistry, The Pennsylvania State University, University Park, Pennsylvania 16802, Center for Biophysics and Computational Biology, University of Illinois, Urbana, Illinois 61801, and Institute of Bioorganic Chemistry, Polish Academy of Sciences, Z. Noskowskiego 12/14, 61-704 Poznañ, Poland

Received August 17, 2004; Revised Manuscript Received August 26, 2004

ABSTRACT: Modified nucleotides allow fundamental energetic and kinetic properties of nucleic acids to be probed. Here, we demonstrate that an RNA hairpin containing the nucleotide analogue 8-bromoguanosine (8BrG or ***G***), gcUUC***G***gc, has enhanced stability relative to the unmodified hairpin, with $\Delta\Delta G^\circ_{37} = -0.69 \pm 0.15$ kcal mol^{-1} and $\Delta T_M = +6.8 \pm 1.4$ °C. NMR spectroscopic data suggest that the enhanced stability of gcUUC***G***gc does not arise from the native state; laser temperature-jump experiments support this notion, as gcUUCGgc and gcUUC***G***gc have similar unfolding rate constants, but the folding rate constant of gcUUC***G***gc is 4.1-fold faster at 37.5 °C and 2.8-fold faster under isoenergetic conditions. On the basis of these findings, we propose that 8BrG reduces the conformational entropy of the denatured state, resulting in an accelerated conformational search for the native state and enhanced stability.

Interactions among RNA nucleotides result in the rapid formation of secondary structure, typically in a few microseconds (*1*); tertiary structure subsequently develops more slowly, typically in seconds to minutes, through the interaction of secondary structural elements (for example, see refs *2*−*6*), although exceptions to this folding succession have been noted (*7*−*10*). This folding hierarchy results in linkage between the equilibria for secondary and tertiary structure formation (Figure 1). Hierarchical folding is the result of several fundamental features of RNA energetics including the strongly favorable thermodynamics of stacking and hydrogen bonding in secondary structure formation, the rapid kinetics of secondary structure formation relative to tertiary structure formation, and in vivo folding being cotranscriptional such that secondary structures are synthesized before distal tertiary elements, and thus can fold first (*11*−*13*). In addition, tertiary structure generally involves the assembly of *preformed* secondary structural elements.

Many of the fundamental principles of RNA folding at both the secondary and tertiary structure levels have yet to be elucidated. In particular, the role of the denatured state and the temperature dependence of folding, especially involving non-Arrhenius kinetics, are under intense investigation for secondary and tertiary structures alike (*14*−*19*). Because the processes of secondary and tertiary structure formation are linked, insight into the kinetics of secondary structure formation may aid our understanding of the overall pathway for tertiary structure formation.

To gain insight into these issues, we chose to study the folding kinetics of a well-characterized, unusually stable RNA secondary structure, the UUCG tetraloop (*20*−*23*). The YNMG hairpin motif, which includes the UUCG tetraloop, has a *syn*-G at position 4 of the loop that is involved in stacking and hydrogen bonding (*24*−*27*). Substitution of bulky substituents such as Br for G H8 (8BrG or ***G***),[1] limits rotation about the glycosidic bond and disfavors the *anti* conformation, which would require that Br reside over ribose, resulting in an equilibrium shift of $\Delta G^\circ_{37} \approx 2$ kcal mol^{-1} (*28*, *29*). In addition, the modified nucleotide 8BrG adopts the *syn* conformation in a crystal structure of the nucleoside (*30*−*32*).

The utility of 8BrG for controlling the folding of G-quartets (*33*) and YNMG hairpins (*29*) has been previously demonstrated. Specifically, incorporation of deoxy-8BrG into *syn* positions of G-quartets was stabilizing by $\Delta\Delta G^\circ_{25} = -0.6$ to -1.1 kcal mol^{-1}, while incorporation into *anti*

† The organizations that supported this work with the following grants, awards, and fellowships are gratefully acknowledged: NSF Grant MCB-0316925 to H.M. and M.G., NSF Grant MCB-9984129, a Fellowship from the Alfred P. Sloan Foundation, and a Camille Dreyfus Teacher-Scholar Award to P.C.B., NIH Grant 1R03 TW1068-01 to R.K. and D. H. Turner, and PZB-KBN Grant 059/T09/14 to R.K.

* To whom correspondence should be addressed. Phone: (814) 863-3812 (P.C.B.); (217) 333-1624 (M.G.). Fax: (814) 863-8403 (P.C.B.); (217) 244-3186 (M.G.). E-mail: pcb@chem.psu.edu (P.C.B.); gruebele@scs.uiuc.edu (M.G.).

‡ The Pennsylvania State University.

§ University of Illinois at Urbana-Champaign.

|| Polish Academy of Sciences.

[1] Abbreviations: 8BrG or ***G***, 8-bromoguanosine; C_T, strand concentration; cYNMGg, the hairpin loop sequence is capitalized, N = A, C, G, or U, M = A or C, and Y = C or U; $\Delta\delta$, change in the chemical shift in parts per million (ppm); f_F, fraction folded; f_U, fraction unfolded; K_{37}, equilibrium constant for folding at 37 °C; k_1, folding rate constant; k_{-1}, unfolding rate constant; L_n, hairpin loop nucleotide *n*; nt, nucleotide; $P_{10}E_{0.1}$, 10 mM sodium phosphate and 0.1 mM disodium ethylenediaminetetraacetic acid (EDTA) at pH 7.1; TEMED, *N*,*N*,*N*′,*N*′-tetramethylethylenediamine; *T*-jump, temperature jump; T_M, denaturation temperature.

10.1021/bi048213e CCC: $27.50
Published on Web 10/16/2004

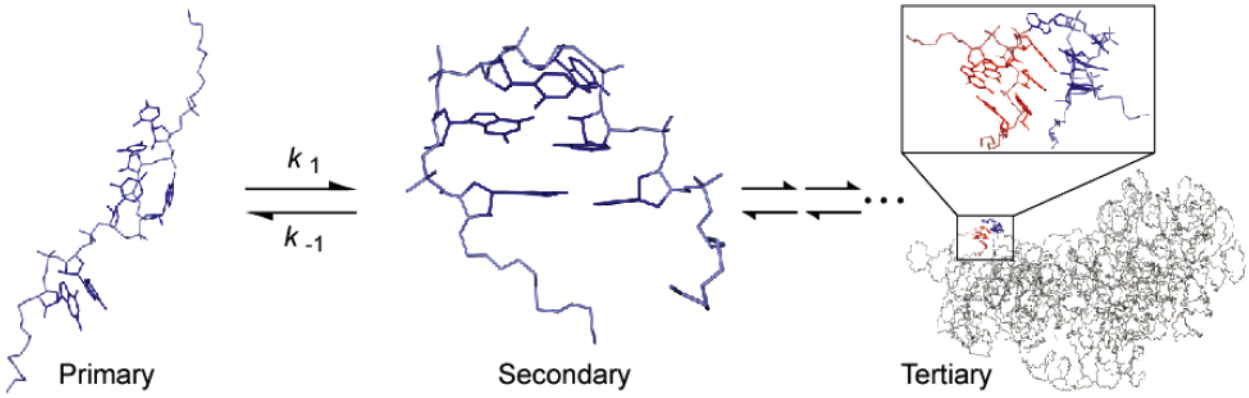

FIGURE 1: Depiction of the hierarchical folding of RNA. Primary and secondary structures are in rapid equilibrium, having rate constants for secondary structure folding, k_1, and unfolding, k_{-1}, that are typically much faster than for tertiary folding. The hairpin secondary structure is also depicted in equilibrium with a larger tertiary structure. The stability, rate of formation, and propensity of the secondary structure to misfold affect the tertiary structure (and vice-versa) due to the linked nature of the equilibria. The secondary structure shown is the UUCG tetraloop from the X-ray crystal structure of 30S rRNA [PDB entry 1J5E (*87*)]. For the sake of clarity, bases are omitted for all residues except the UUCG and GAAA tetraloops. The tertiary structure illustrates the interaction between the UUCG tetraloop [blue, residues 343−346 using numbering from *Escherichia coli* (*88*)] and a GAAA tetraloop (red, residues 159−162).

positions was destabilizing by +0.8 to +1.0 kcal mol^{-1} (*33*). Incorporation of 8BrG at position 4 of YNMG hairpins revealed a significant destabilization of the alternative duplex conformation ($\Delta\Delta G^\circ_{37} \approx +4.7$ kcal mol^{-1} or +2.4 kcal mol^{-1} (base pair)$^{-1}$) (*29*). These findings suggested that site-specific incorporation of 8BrG favors the hairpin conformation in a hairpin−duplex equilibrium primarily by *destabilizing* the duplex conformation, in which bases adopt the *anti* glycosidic conformation. Interestingly, thermal denaturation studies of 12 nt 8BrG-substituted YNMG sequences suggested that 8BrG substitution might also afford a small *stabilization* of the hairpin conformation ($\Delta\Delta G^\circ_{37} = -0.1 \pm 0.2$ to -0.6 ± 0.1 kcal mol^{-1}) (*29*), which motivated the characterization presented here.

To provide further insight into the energetics and kinetics of hairpin formation, unmodified and 8BrG-substituted gcUUCGgc tetraloops (the loop sequence is capitalized) have been characterized by UV and NMR thermal denaturation and laser temperature-jump (*T*-jump) spectroscopy. Unmodified and 8BrG-substituted ggUUCGcc tetraloops, which adopt a structurally related, UUCG-like hairpin of lesser stability (*34*), have also been characterized in an effort to gain insight into the kinetic origin of the unusual stability of a CG closing base pair.

MATERIALS AND METHODS

Synthesis of 8BrG Phosphoramidite and Preparation of RNA. For thermodynamic, structural, and kinetic studies, unmodified 8 and 12 nt synthetic RNA oligonucleotides were from Dharmacon Research. Oligonucleotides were deprotected at 60 °C for 30 min in 100 mM acetic acid and TEMED (pH 3.8), dried in vacuo, and desalted using Sep-Pak Plus C18 cartridges (Waters). Detailed procedures for the synthesis of the 8BrG phosphoramidite and 8BrG-substituted RNA oligonucleotides have been described (*29*, *35*). Mass spectroscopy has shown that 8BrG remains intact during thermal denaturation experiments (*29*).

RNA oligonucleotides were stored in $P_{10}E_{0.1}$ [10 mM sodium phosphate, 0.1 mM Na_2EDTA, pH 7.1] for UV thermal denaturation, NMR, and laser *T*-jump experiments. Low-salt buffers were used to favor the hairpin conformation (*21*, *29*, *36*, *37*). For NMR and *T*-jump experiments, hairpins were renatured by heating into the unfolded baseline for all sequences studied (typically 70 °C for 8 nt hairpins and 90 °C for 12 nt hairpins) for 1 min, followed by rapid cooling to disfavor nonnative conformations.

RNA concentrations were determined using absorbance values for the denatured state at 90 °C with extinction coefficients from a nearest-neighbor analysis (*38*, *39*). The extinction coefficient for 8BrG was assumed to be identical to that of G (*29*); any errors introduced from this assumption should be negligible since the equilibrium was independent of concentration.

Overview of Unfolding Experiments. Thermodynamic parameters are from thermal denaturation experiments using detection by UV and NMR spectroscopies (Table 1). Measurements of UV absorbance as a function of temperature comprised the largest and most complete data set, with data collected every 0.5 °C between 5 and 95 °C, which facilitated the determination of slopes and intercepts for the native and unfolded baselines of the sigmoidal transition. Phosphorus NMR spectroscopy was also used to collect the chemical shift difference as a function of temperature and helped test the two-state nature of the folding transition; however, this method did not provide sufficiently long native and unfolded baselines to accurately determine thermodynamic parameters independently. Consequently, thermodynamic parameters for NMR data were determined by global fitting of the temperature dependence of chemical shift differences (relative to phosphate) for the seven ^{31}P resonances together with absorbance at 260 and 280 nm from six UV data sets. Global fits were by nonlinear least-squares regression using the Marquardt−Levenburg algorithm in Savuka version 5.2.7 (*40*, *41*). The slope and intercept of the native and unfolded baselines for the UV data sets were determined independently and were subsequently fixed during global fitting. The enthalpy and melting temperature were linked between the NMR and UV data sets (i.e., forced to give a single ΔH° and T_M for all seven NMR and six UV data sets) while the NMR native and unfolded baselines were allowed to vary. Outcomes for fits to UV-only and UV plus NMR data are listed in Table 1.

UV Spectroscopy and Thermal Denaturation. Thermodynamic parameters from UV unfolding experiments were

Table 1: Thermodynamic Parameters for Hairpin Formation[a]

sequence[b]	ΔH° [c] (kcal mol^{-1})	ΔS° [c] (eu)	ΔG°_{37} [c] (kcal mol^{-1})	$\Delta\Delta G^\circ_{37}$ [d,e] (kcal mol^{-1})	T_M [e] (°C)	ΔT_M [f] (°C)
12 nt UUCG	−47.7 ± 0.9	−138.4 ± 2.5	−4.81 ± 0.11		71.8	
12 nt UUUU	−38.7 ± 1.4	−116.5 ± 4.4	−2.60 ± 0.11	+2.21 ± 0.16	59.2	−12.6
gcUUCGgc	−24.2 ± 0.5	−74.9 ± 1.7	−0.97 ± 0.12		49.9	
	−26.7 ± 0.2	*−82.7* ± 0.2	*−1.05* ± 0.28		*49.7*	
gcUUC***G***gc	−27.7 ± 0.7	−84.0 ± 2.4	−1.66 ± 0.08	−0.69 ± 0.15	56.7	+6.8
	−27.9 ± 0.2	*−84.9* ± 0.2	*−1.57* ± 0.28	*−0.52* ± 0.40	*55.5*	*+5.8*
ggUUCGcc	−18.4 ± 0.5	−61.2 ± 1.3	0.57 ± 0.06		27.7	
ggUUC***G***cc	−20.3 ± 1.1	−66.1 ± 3.3	0.24 ± 0.08	−0.32 ± 0.10	33.3	+5.5

[a] Parameters are from denaturation experiments in $P_{10}E_{0.1}$ (pH 7.1). For UV data, parameters are the average of ≥3 independently prepared samples fit to a two-state model with sloping baselines. Other parameters (italics) are from global fits of UV data combined with the temperature dependence of NMR chemical shift differences for the seven observed ^{31}P resonances (Materials and Methods). [b] The loop sequence is capitalized, and the 8BrG substitution is bold and italic (***G***). The 12 nt sequences are of the type 5′-GGAC $L_1L_2L_3L_4$ GUCC, where L_n corresponds to loop nucleotide *n*. [c] Errors for ΔH°, ΔS°,and ΔG°_{37} values are standard deviations from repeated experiments (UV data) or global fits (UV and NMR data). An extra significant figure is provided to minimize rounding errors in calculations. [d] Errors in $\Delta\Delta G^\circ_{37}$ were propagated from ΔG° values by standard methods (*44*). [e] Estimated errors in T_M are ±1 °C. [f] Values for $\Delta\Delta G^\circ_{37}$ and ΔT_M are relative to those of unmodified sequences for 8BrG-substituted 8 nt sequences and to 12 nt UUCG for 12 nt UUUU.

obtained at 260 and 280 nm in 1 cm path length cuvettes with a heating rate of ∼1.0 °C min^{-1} using a Gilford Response II spectrophotometer equipped with a temperature controller. To favor the hairpin conformation, the RNA was renatured prior to each experiment by heating to 95 °C, followed immediately by a refolding experiment from 95 to 5 °C. Subsequent denaturation experiments were from 5 to 95 °C or from 95 to 5 °C, and were carried out successively. Overlapping curves were obtained, consistent with reversibility of the transition (Supporting Information Figure 1). Thermodynamic parameters were obtained at strand concentrations (C_T) between 1 and 25 μM. The similarity of unfolding transitions over a range of C_T up to ∼250-fold (from UV data acquired at ≤25 μM and NMR data acquired at ≥250 μM) was consistent with the unfolding transition being due to the hairpin rather than duplex species. Formation of the hairpin conformation at these concentrations has also been confirmed by the presence of unique NMR spectral features for the hairpin conformation (Supporting Information Figure 2) (*21*, *24*), and it has been shown that the hairpin conformation is further favored by 8BrG substitution (*29*).

Thermodynamic parameters from UV thermal denaturation were determined by nonlinear curve fitting using a set of parametric equations for a two-state, unimolecular transition defined in KaleidaGraph (Synergy Software, Reading, PA) (*42*, *43*), as shown in eqs 1 and 2,

$$\text{signal} = (m_U T + b_U) + [(m_F T + b_F) - (m_U T + b_U)]K/(1 + K) \quad (1)$$

$$K = \exp[\Delta H/R(1/T_M - 1/T)] \quad (2)$$

where T is the temperature (K), m_U and b_U are the unfolded baseline slope and intercept, respectively, m_F and b_F are the folded baseline slope and intercept, respectively, K is the folding equilibrium constant from Figure 1 (left), ΔH is the enthalpy for hairpin formation, $R = 1.987 \times 10^{-3}$ kcal mol^{-1} K^{-1}, and T_M is the hairpin melting temperature (K). These equations are based on the assumption that the observed signal is the weighted average of the signals of two states, S_F and S_U:

$$\text{signal} = S_F f_F + S_U f_U \quad (3)$$

where S_F and S_U are signals from the folded and unfolded states, respectively, and f_F and f_U are the fractions of folded and unfolded molecules, respectively. ΔH° and T_M values were determined directly from fits of the primary thermal denaturation data, and ΔS° and ΔG°_{37} were determined using standard thermodynamic relationships. For each set of thermodynamic parameters determined by UV thermal denaturation, ≥3 independent experiments were averaged. Errors in ΔH°, ΔS°, and ΔG°_{37} were statistical errors for nonlinear curve fitting from combined NMR- and UV-derived data, or the standard deviations of ≥3 experiments from only UV-derived data; errors in ΔG°_{37} were propagated by standard methods (Table 1) (*44*).

Phosphorus NMR Spectroscopy and Thermal Denaturation. RNA oligonucleotides were suspended in 95% H_2O and 5% ^2H_2O (v/v) with $P_{10}E_{0.1}$ (pH 7.1). Thermodynamic parameters from NMR unfolding experiments were obtained from the temperature dependence of the chemical shift ($\Delta\delta$, ppm) for each RNA phosphorus resonance relative to that of $P_{10}E_{0.1}$ (seven resonances per hairpin). These measurements relied upon the assumption that the RNA was in the fast exchange regime for switching between the hairpin and denatured conformations; this assumption was supported by *T*-jump measurements (Table 2). To be in the fast exchange regime for NMR spectroscopy, τ^{-1} must satisfy eq 4, where

$$\tau^{-1} \gg 2\pi(\nu_A - \nu_B) \quad (4)$$

ν_A and ν_B are the chemical shifts (Hz) of a given atom in conformations A and B, respectively (*45*). For ^{31}P NMR data in the folded and denatured temperature regimes, the chemical shift change between the hairpin and denatured conformations of gcUUCGgc and gcUUC***G***gc was ≤1.5 ppm (Supporting Information Figure 2). Thus, according to eq 4, τ^{-1} must be much greater than 1.9×10^3 s^{-1} (=2π(1.5 ppm)(202 Hz ppm^{-1})) for the fast exchange regime to exist; this condition is satisfied by all the relaxation rate constants reported here, in which $\tau^{-1} \geq 1.9 \times 10^4$ s^{-1} (Table 2). The appearance of only seven resonances at all temperatures and the sigmoidal temperature dependence of the chemical shifts also support fast exchange.

NMR data were collected on a Bruker AMX2-500 spectrometer at 202 MHz (^{31}P) using a 5 mm inverse broad-

Table 2: Kinetic Parameters for Hairpin Formation at 37.5 or 65 °C and Isoenergetic Conditions[a]

sequence[b]	[RNA][c] (mM)	T_M (°C)	T^u (°C)	f_F[d]	$\tau^{-1} \times 10^{-4}$ (s^{-1})	$k_1 \times 10^{-4}$ [e] (s^{-1})	$k_{-1} \times 10^{-4}$ [e] (s^{-1})
12 nt UUCG		71.8	72.5	0.45	11.0 ± 0.1	4.9	6.1
			65.0	0.79	7.7 ± 0.1	6.1	1.6
12 nt UUUU		59.2	60.0	0.46	18.9 ± 0.5	8.7	10.3
			65.0	0.26	17.3 ± 0.3	4.5	12.8
gcUUCGgc	4.6	49.9	50.0	0.50	13.1 ± 0.3	6.5	6.6
			37.5	0.82	8.2 ± 0.2	6.7	1.5
gcUUC***G***gc	3.9	56.7	57.5	0.47	38.5 ± 1.0	18.2	20.3
			37.5	0.93	29.2 ± 3.1	27.2	2.0
ggUUCGcc	0.9	27.7	27.5	0.48	1.9 ± 0.1	0.9	0.9
			37.5	0.27	4.8 ± 0.3	1.3	3.5
ggUUC***G***cc	2.8	33.3	32.5	0.54	8.9 ± 0.3	4.8	4.1
			37.5	0.41	11.6 ± 0.4	4.7	6.9

[a] Kinetic parameters were calculated using equilibrium constants (Table 1) and relaxation rates determined at the temperatures indicated ($\sim T_M$ and 37.5 °C or 65 °C); these were the solution temperatures immediately following absorption of the heating laser pulse. It is worth noting that for isoenergetic conditions ($\Delta G = 0$), $k_1 = k_{-1}$ at $T = T_M$. Slight discrepancies between k_1 and k_{-1} at $T \approx T_M$ are attributed to small differences between T and T_M for these experiments. [b] The loop sequence is capitalized, and the 8BrG substitution is bold and italic (***G***). The 12 nt sequences are 5′-GGAC $L_1L_2L_3L_4$ GUCC, where L_n corresponds to loop nucleotide n. [c] RNA concentrations were determined as described in the Materials and Methods. [d] The fraction folded, f_F, was calculated from $K/(K + 1) = k_1/(k_1 + k_{-1})$. Likewise, the fraction unfolded, f_U, was calculated from $1/(K + 1) = k_{-1}/(k_1 + k_{-1})$; K values are derived from Table 1. [e] Rates were determined from the observed relaxation rate (τ^{-1}) and folded or unfolded populations: $\tau^{-1} = k_1/f_F = k_{-1}/f_U$. Thus, when f_F is near unity, $\tau^{-1} \approx k_1$, and when f_F is near zero, $\tau^{-1} \approx k_{-1}$. Errors are from single-exponential fits of the data (Figures 3 and 4).

band probe. RNA concentrations for NMR experiments ranged from 0.9 to 4.6 mM C_T. Following renaturation, the RNA was allowed to equilibrate at the experimental temperature until a constant lock signal was obtained. Spectra were acquired in 3 °C increments from 14 to 74 °C for gcUUCGgc and from 13 to 79 °C for gcUUC***G***gc using a spectral width of 3049 Hz, a 3 s recycle delay, and proton decoupling (WALTZ-16) (*46*). Spectra were referenced to 85% H_3PO_4 at 0.0 ppm contained in an internal coaxial tube. Temperatures inside the NMR tube were calibrated by comparing the temperature dependence of the chemical shift difference between (m)ethyl and hydroxyl functional groups from ethylene glycol (for temperatures ≥25 °C) and methanol (for temperatures ≤25 °C) to a standard curve (*47*). Free induction decays were zero-filled and apodized with 1 Hz line broadening using XWINNMR (Bruker).

Laser Temperature-Jump Kinetics Measurements. General considerations for the construction and implementation of a Raman laser *T*-jump apparatus have been described (*48*−*51*), and several examples exist of the application of *T*-jump for the study of DNA and RNA folding (*14*, *52*−*56*). The Raman laser *T*-jump apparatus used in this study was loosely based upon a similar apparatus described previously (*50*, *51*, *57*−*62*). Briefly, kinetics were initiated by a 10 ns, 1.54 μm heating pulse derived from Raman shifting an 800 mJ Q-switched Nd:YAG laser in high-pressure CH_4 gas. A 50/50 beam splitter produced two counterpropagating heating pulses at the sample cell to yield a more homogeneous longitudinal heating profile.

The average of the temperature-jump size was 7.5 °C, calibrated by observing tryptophan fluorescence measurements, as previously described (*59*). Tryptophan fluorescence was measured at the equilibrium temperature (e.g., 30 °C) before the *T*-jump and afterward at the equilibrium temperature plus the *T*-jump size (e.g., 7.5 °C, yielding a post-*T*-jump temperature of 37.5 °C). Next, the Nd:YAG laser was blocked, and a steady-state fluorescence at the pre-*T*-jump temperature was collected. The equilibrium temperature was then increased until the steady-state fluorescence was identical to the post-*T*-jump fluorescence; the equilibrium temperature difference was the *T*-jump size.

Cylindrical quartz cells (Hellma) with a 100 μm path length were used to facilitate minimization of both sample volume and heating artifacts. The sample temperature before the temperature jump was controlled by a circulating heat bath and fine-tuned to ±0.1 °C by a thermoelectric element driven by a temperature controller (Lakeshore 330) with a diode feedback sensor. RNA was in $P_{10}E_{0.1}$ (pH 7.1), and concentrations for laser *T*-jump spectroscopy measurements ranged from 0.9 to 4.6 mM C_T. Extremely fast absorbance changes were observed and likely correspond to unstacking or other rapid conformational changes (*63*); these conformational changes typically accounted for <1/3 of the total absorbance change. Furthermore, these changes were probably not due to small changes in buffer absorbance following a 7.5 °C *T*-jump since the temperature dependence of the $P_{10}E_{0.1}$ absorbance was $\leq 5 \times 10^{-5}$ AU/°C. Alternatively, these absorbance changes may be a consequence of residual lensing effects from refractive index changes caused by uneven heating of the solution.

Laser UV light at 280 nm was used as the probe beam. The 14 ns spaced UV pulse train was generated from a frequency-tripled mode-locked Ti:sapphire laser, as described (*50*, *59*). The UV beam was gated onto the sample cell, absorbed by the sample, and focused by a lens onto a fast photomultiplier (MCT) detector (Hamamatsu R5600). Multiple band-pass filters were placed in front of the detector to filter out unwanted scattered light. The signal was digitized by a transient digitizer (Tektronix) with a 500 ps time resolution and a 100 MHz bandwidth.

Relaxation curves following a 10 ns laser *T*-jump were obtained by following the amplitude of each pulse in 14 ns steps out to several hundred microseconds; the detected signal was proportional to the percent transmittance (%*T*). Transmittance traces were converted into absorption traces (ΔAbs), and relaxations time constants were determined with the fitting program IGOR (WaveMetrics) using single-exponential (eq 5, where a_1 is the absorbance immediately following

$$a(t) = \chi_1 a_1 + (1 - \chi_1) a_2 \quad (5)$$

the *T*-jump, a_2 is the absorbance after equilibration at the higher temperature, and χ_1 indicates the progress toward equilibrium, with $\chi_1 = 1$ just after the *T*-jump and $\chi_1 = 0$ for the equilibrated system) or double-exponential functions for all sequences. A single exponential is consistent with a simple two-state model; if the system populates more than two states, deviation from single-exponential behavior occurs (*49*, *59*, *64*, *65*).

For a two-state process (Figure 1), the forward (k_1) and reverse (k_{-1}) folding rate constants are related to the observed relaxation lifetime ($\tau = k_{obs}^{-1}$) by eq 6, and to the equilibrium constant for hairpin formation (*K*) by eq 7. Thus, experimental determination of τ^{-1} from *T*-jump and *K* from thermal denaturation experiments provides a means for determination of individual k_1 and k_{-1} values (Table 2).

$$\tau^{-1} = k_{obs} = k_1 + k_{-1} \quad (6)$$

$$K = k_1/k_{-1} \quad (7)$$

RESULTS

Design of the Hairpin Model Systems. We previously studied the structure and stability of 12 nt YNMG hairpins in the context of a four base pair stem (*24*, *29*). The hairpins used in the present study include 12 nt hairpins with UUCG and UUUU loop sequences, as well as 8 nt UUCG tetraloops. It was necessary to measure certain rate constants with the 12 nt tetraloops because the 8 nt UUUU tetraloop was exceedingly unstable and it was not possible to obtain a complete folded baseline above 0 °C for this RNA. The shorter 8 nt UUCG hairpins are closed by a CG or GC base pair, with stems that are only two base pairs long. The choice of two base pair stems was inspired by several studies that showed these shortened sequences assume stable, well-folded UNCG-like tetraloops regardless of penultimate base pair identity (*66*−*69*). Also, two base pairs is the minimum stem length capable of hairpin formation (*66*−*69*). Two base pair stems were chosen for three reasons. First, we wished to minimize multiple pathways for helix nucleation with the intention of making folding more dependent upon loop organization. Second, we wanted to avoid alternative pairings; the absence of significant alternative pairings is supported by free energy minimization calculations using mfold 3.1 with a window parameter of zero and a 100% suboptimality (*70*, *71*). These calculations did not return suboptimal structures for any of the sequences under investigation. Third, we sought to provide lower melting temperatures, ∼50 °C and ∼70 °C for 8 and 12 nt YNMG hairpins, respectively. This reduced stability afforded long folded and unfolded baselines in thermal denaturation experiments, improving the accuracy of thermodynamic parameters. These T_M values also produced significant absorbance changes in *T*-jump experiments near physiologically relevant temperatures.

In an effort to determine whether unmodified, unusually stable tetraloops derive their stability from faster folding or slower unfolding, *T*-jump data were also collected for 12 nt UUCG and UUUU tetraloops. Also, the UUCG tetraloop closing base pair was varied between the more stable CG and less stable GC to examine the kinetic basis of exceptional stability for the CG closing base pair.

Evidence for Two-State Unfolding of Hairpins. To confirm the structural relatedness and two-state folding of YNMG hairpins, ^{31}P NMR experiments were carried out on gcUUCGgc and gcUUC***G***gc. Seven resonances were observed for both gcUUCGgc and gcUUC***G***gc, as expected (Supporting Information Figure 2). In addition, observed spectra for the two hairpins at $T \ll T_M$ were similar to each other and to reported profiles for the UUCG tetraloop conformation (e.g., see refs *21*, *29*, and *34*) with a disperse spectrum spread over >1.5 ppm and a resonance shifted downfield to ∼1 ppm (Supporting Information Figure 2); these data support the notion that 8-Br substitution does not affect the folded state, similar to findings for 12 nt sequences (*29*).

Representative unfolding transitions for unmodified and 8BrG-substituted gcUUCGgc hairpins were obtained from temperature-dependent changes in UV absorbance and NMR chemical shift difference (Figure 2A,B). Data from UV and NMR thermal denaturation experiments yielded sigmoidal species plots (Figure 2C,D) and similar thermodynamic parameters for hairpin formation (Table 1), consistent with two-state behavior. Furthermore, single relaxation lifetimes observed in laser *T*-jump experiments at the hairpin melting temperatures were consistent with two-state behavior, as was the absence of additional resonances in ^{31}P NMR experiments. On the basis of these experiments, data were treated with eqs 1−3, 6, and 7 to extract values for k_1 and k_{-1}.

It is worth noting that, although consistent with two-state behavior at physiological and melting temperatures, our data cannot rule out the existence of a poorly populated or spectroscopically silent conformation, such as a globular intermediate proposed for a GCAA tetraloop on the basis of simulations (*72*, *73*).

Thermodynamic Measurements of Hairpin Folding. As expected (*36*, *74*), the 12 nt UUCG hairpin was very stable, with ΔG°_{37} and T_M values of −4.81 ± 0.11 kcal mol^{-1} and 71.8 °C, respectively; in contrast, the 12 nt UUUU hairpin was significantly less stable with ΔG°_{37} and T_M values of −2.60 ± 0.11 kcal mol^{-1} and 59.2 °C, respectively (Table 1). The difference in loop free energy of −2.21 ± 0.16 kcal mol^{-1} is similar to published data (*36*).

For 8 nt sequences, gcUUCGgc had ΔG°_{37} and T_M values of −0.97 ± 0.12 kcal mol^{-1} and 49.9 °C, respectively, while gcUUC***G***gc had ΔG°_{37} and T_M values of −1.66 ± 0.08 kcal mol^{-1} and 56.7 °C, respectively (Table 1). Apparently, substitution of 8BrG for G at position 4 of the UUCG tetraloop in the context of a stable CG closing base pair results in a significant stabilization of the loop, with $\Delta\Delta G^\circ_{37}$ = −0.69 ± 0.15 kcal mol^{-1} and ΔT_M = 6.8 °C. Free energy and T_M values for gcUUCGgc are similar to previously reported values of −1.5 kcal mol^{-1} and 54.4 °C (*66*−*69*). The small discrepancy may be due to differences in the ionic strength of the buffers used; currently, little is known about the salt dependence of hairpin stability. For gcUUCGgc and gcUUC***G***gc, a $\Delta\Delta G^\circ_{37}$ for of −0.69 kcal mol^{-1} corresponds to a K_{37}(8BrG)/K_{37}(G) ratio of 3.1.

For the 8 nt tetraloop, the GC closing base pair of ggUUCGcc had ΔG°_{37} and T_M values of 0.57 ± 0.06 kcal mol^{-1} and 27.7 °C, respectively, while ggUUC***G***cc had ΔG°_{37} and T_M values of 0.24 ± 0.08 kcal mol^{-1} and 33.3 °C, respectively (Table 1). Thus, substitution of 8BrG for G at

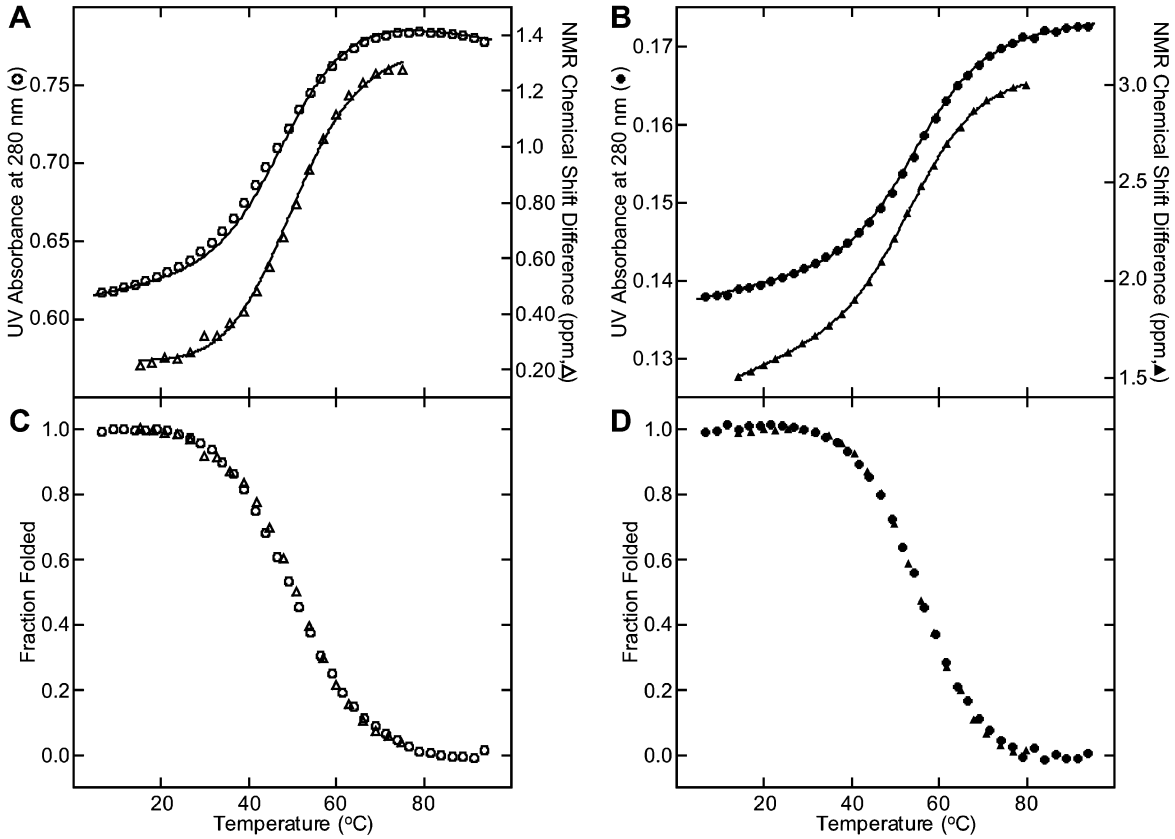

FIGURE 2: Spectroscopic evidence for two-state unfolding of the gcUUCGgc and gcUUC***G***gc hairpins. Representative thermal denaturations of **(**A**)** gcUUCGgc (empty symbols) and (B) gcUUC***G***gc (filled symbols) obtained using UV (circles) and NMR (triangles) spectroscopic probes. UV absorbance data were collected at 280 nm every 0.5 °C from 5 to 95 °C in $P_{10}E_{0.1}$ for gcUUCGgc (○) an gcUUC***G***gc (●); only every fifth data point is shown for clarity. NMR chemical shift difference data (triangles) (relative to internal phosphate) for G7 (assigned on the basis of comparison to ref *21*), the most downfield shifted resonance (● in Supporting Information Figure 2). The ^{31}P resonance as a function of temperature was collected every 3 °C from 14 to 74 °C for gcUUCGgc (△) and 13−79 °C for gcUUC***G***gc (▲). The increase in absorbance and decrease in chemical shift differences among seven resonances with temperature are consistent with denaturation of the tetraloops. Fraction folded as a function of temperature for **(**C) gcUUCGgc and (D**)** gcUUC***G***gc. Overlapping sigmoidal transitions using the different measurement techniques are consistent with two-state behavior.

position 4 of a UUCG tetraloop closed by the less stable GC closing base pair resulted in loop stabilization with $\Delta\Delta G^\circ_{37} = -0.32 \pm 0.10$ kcal mol^{-1} and $\Delta T_M = 5.5$ °C; these values, though significant, are somewhat less than for gcUUCGgc (Discussion). The T_M value of 27.7 °C for ggUUCGcc is similar to a previously determined value of ∼24 °C for cgUUCGcg (*66*). Changing the closing base pair from CG to GC was destabilizing by $\Delta\Delta G^\circ_{37} = 1.54 \pm 0.13$ kcal mol^{-1} and $\Delta T_M = -22.2$ °C for ggUUCGcc, and $\Delta\Delta G^\circ_{37} = 1.90 \pm 0.11$ kcal mol^{-1} and $\Delta T_M = -23.4$ °C for ggUUC***G***cc.

Laser Temperature-Jump Kinetics Measurements of Hairpin Folding. Relaxation profiles exhibited a single relaxation time that was independent of concentration over the temperatures considered here (37.5 °C and near the T_M of each hairpin, Table 2), consistent with a unimolecular relaxation as expected for a hairpin. Deviations that are best described by multiple relaxation times were observed at very high and low temperatures (Supporting Information Figure 3), and will be presented elsewhere. Typical absorbance relaxation profiles for gcUUCGgc and gcUUC***G***gc are depicted in Figure 3.

Comparison of 12 nt tetraloops for UUCG and UUUU at 65.0 °C revealed that for UUCG folding is 1.4-fold faster while unfolding is 8.0-fold slower (Table 2). Apparently, the greater stability of the UUCG tetraloop has its kinetic origin primarily in slower unfolding rather than faster folding. Similarly, comparisons near $\Delta G = 0$ (i.e., isoenergetic conditions; $f_F \approx 0.50$) revealed that UUCG folds and unfolds 1.8-fold slower than UUUU. In summary, the kinetic origins of loop destabilization, as demonstrated by switching the UUCG tetraloop to UUUU, were found almost exclusively in k_{-1}, the rate constant for unfolding of the native state.

For the shorter 8 nt hairpins, gcUUC***G***gc folds 4.1-fold *faster* than gcUUCGgc at 37.5 °C, similar to the ratio of K values, causing the rates of unfolding to be nearly identical. Likewise, near $T = T_M$ ($f_F \approx 0.50$) gcUUC***G***gc folds and unfolds ∼3-fold faster than gcUUCGgc. These novel results are consistent with the greater stability of gcUUC***G***gc having its origin in faster folding.

Changing the closing base pair of the UUCG tetraloop from CG to GC only slightly diminished the effect of 8BrG upon the observed rate of folding; ggUUC***G***cc folds 3.6-fold faster than ggUUCGcc at 37.5 °C, while unfolding is affected only 2.0-fold (Figure 4). Also, ggUUC***G***cc folds and unfolds ∼4.9-fold faster than ggUUCGcc near $T = T_M$ ($f_F \approx 0.50$). Thus, the kinetic origin of the enhanced stability of the 8BrG substitution for both CG and GC closing base pairs is unusual in that it arises from faster folding of the denatured state.

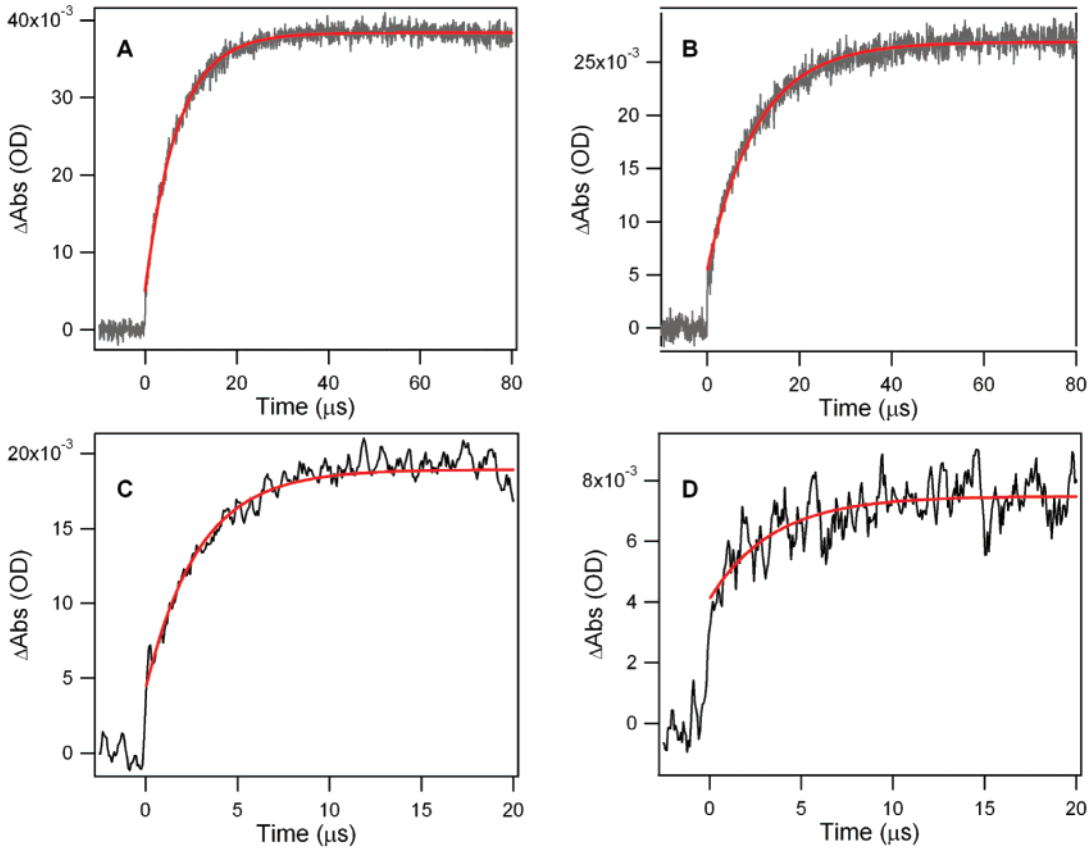

FIGURE 3: Representative relaxations for gcUUCGgc and gcUUC***G***gc after 7.5 °C *T*-jumps. At time 0, a *T*-jump was applied **(**A) from 42.5 to 50.0 °C (∼T_M) and (B**)** from 30.0 to 37.5 °C for 4.6 mM gcUUCGgc. Similarly, at time 0 a *T*-jump was applied **(**C**)** from 50.0 to 57.5 °C (∼T_M) and **(**D**)** from 30 to 37.5 °C for 3.9 mM gcUUC***G***gc. Relaxation traces were fit to single exponentials (red lines). Note the different time scales. It is also worth noting that it is possible to fit the same data in panel B using a double-exponential function to reveal a fast phase; this was a common circumstance when the temperature was far from the T_M.

Finally, comparison at 37.5 °C of gcUUCGgc with ggUUCGcc, and gcUUC***G***gc with ggUUC***G***cc, reveals that the kinetic origin of enhanced stability for the CG closing base pair derives from both faster folding (5.2−5.8-fold larger k_1) and slower unfolding (2.3−3.5-fold smaller k_{-1}). It appears that faster folding can drive the stability of modified and unmodified sequences alike.

DISCUSSION

Incorporation of the modified nucleotide 8BrG into RNA hairpins having the YNMG motif resulted in stabilization by folding rate enhancement. Specifically, ΔG°_{37} increased by 0.3−0.7 kcal mol^{-1} and T_M by 6−7 °C. Furthermore, at 37.5 °C 8BrG substitution enhanced the rate of folding up to 4.1-fold.We propose that 8BrG affects the hairpin stability and folding rate by limiting the number of conformations sampled in the denatured state, thereby reducing the conformational entropy of the hairpin and accelerating the conformational search. In the following sections we present support for this model. Additionally, the biological relevance of modifications at position 8 of purines is discussed, and the possibility that *unmodified*, unusually stable RNA hairpin sequences derive their stability, in part, from increased folding rate constants is considered.

Stabilization of 8BrG-Substituted YNMG Hairpins by Folding Rate Enhancement. In general, folding and unfolding rate constants determined here (Table 2) were in good agreement with values previously reported for RNA and DNA (*1*, *14*, *52*, *56*) and predicted rates from simulations involving RNA hairpins (*72*). Values are similar to those determined for other hairpins; for example, for $A_6C_6U_6$, a poly-C hexaloop closing a 6 AU base pair stem, $k_1 = 2 \times 10^4$ s^{-1} and $k_{-1} = 2.2 \times 10^3$ s^{-1} (at pH 6.9 and 4.2 °C and in 50 mM sodium cacodylate and 1 M NaCl) (*52*).

Enhanced stability of 12 nt UUCG over UUUU is due almost entirely to slower unfolding of the UUCG tetraloop. This is consistent with slower breaking of the greater number of hydrogen-bonding and stacking interactions in the folded UUCG tetraloop (*21*) versus the comparatively unstructured UUUU tetraloop (*75*). Similar effects occur upon simply increasing the number of base pairs in a duplex (*1*, *49*, *76*). Thus, enhanced stability of 12 nt UUCG relative to UUUU can be considered a primarily folded state effect that is likely enthalpic in origin. The kinetic origin of a free energy difference in k_{-1} is common and has been presented elsewhere (*1*, *49*, *76*).

In contrast, comparison between unmodified and 8BrG-substituted hairpins revealed that the kinetic origin of enhanced stability is faster folding. For instance, at 37.5 °C gcUUC***G***gc folds 4.1-fold faster than gcUUCGgc, with the 8BrG sequence actually unfolding 1.3 times *faster*. Similarly, at 37.5 °C ggUUC***G***cc folds 3.6-fold faster than ggUUCGcc, while unfolding only 2.0-fold faster (Table 2). Thus, the kinetic origin of these effects is unconventional in that faster folding of the unfolded state is primarily responsible for the stability enhancements observed upon 8BrG incorporation.

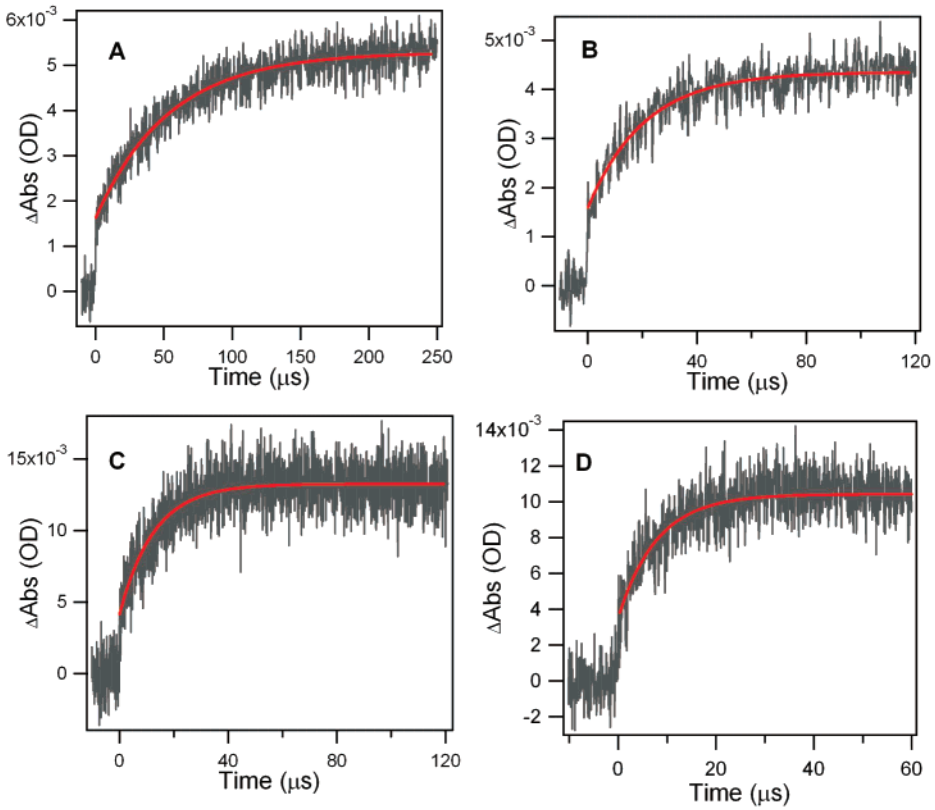

FIGURE 4: Representative relaxations for ggUUCGcc and ggUUC***G***cc after a 7.5 °C *T*-jump. At time 0, a *T*-jump was applied **(**A**)** from 20.0 to 27.5 °C ($\sim T_M$) and **(**B**)** from 30.0 to 37.5 °C for 0.9 mM ggUUCGcc. Similarly, at time 0 a *T*-jump was applied **(**C**)** from 25.0 to 32.5 °C ($\sim T_M$) and **(**D**)** from 30 to 37.5 °C for 2.8 mM ggUUC***G***cc. Relaxation traces were fit to single exponentials (red lines). Note the different time scales.

This effect is likely entropic in origin. Slight acceleration of unfolding by 8BrG incorporation might be due to slightly unfavorable steric effects resulting from the presence of the 8 Br functional group, although one-dimensional NMR experiments did not report any significant changes in the folded state.

At temperatures near or above the T_M of the 8 nt sequences, τ^{-1} approaches k_{-1}. Despite this change, k_1 did not vary significantly, and remained >3-fold faster for 8BrG-substituted versus unmodified hairpins. Unfortunately, it is difficult to describe 8BrG-induced rate constant enhancement at high temperatures ($T \gg T_M$) with any confidence because multiphase folding behavior becomes apparent when $f_F < 0.15$ (Supporting Information Figure 3).

Denatured State in Proteins and Nucleic Acids. Few experimental studies of nucleic acids have described the denatured state in any detail. To understand the denatured state of RNA, it is valuable to consider studies of the denatured state in proteins, and consider those features likely to resemble the denatured state of RNA. Studies of the denatured state for proteins include identification of native-like long-range structure for staphylococcal nuclease through measurement of residual dipolar couplings (*77*). This study suggested that proteins fold to the native conformation from an ensemble of denatured states that possess nativelike structural features. Monte Carlo simulations (*78*−*80*) revealed that biases resulting from steric hindrance and local interactions are a likely candidate for the constraint inherent to the denatured state of biopolymers espoused by Levinthal (*81*). This constraint favors a nativelike conformation that minimizes entropy loss upon folding (*78*). Thus, preorganization of the denatured state can strongly favor folding to the native conformation in proteins and peptides.

As a result of its structure, proline is conformationally limited and has a reduced entropic penalty for the formation of some secondary structures. A study from Raines and coworkers comparing the folding rates of wild-type and modified RNase A revealed that incorporation of the non-natural amino acid 5,5-dimethyl-L-proline (dmP) for a naturally occurring *cis*-proline within a β-turn increases the stability of the protein by accelerating the rate of folding (*82*). Like 8BrG, dmP is sterically constrained; as such it favors the *cis* conformation commonly found in turns. Incorporation of dmP at a position that adopts the *cis* conformation in the native state served to preorganize the denatured state by removing a barrier to folding (*82*). We propose that, like dmP, 8BrG preorganizes the denatured state of RNA, thereby diminishing the entropic penalty for folding and hastening the conformational search for the native state.

Generally, studies of nucleic acid structure have focused on the folded state; there are several reasons for this. Since the biological function of a given RNA typically arises from the folded state, many experiments derive insight from structure−function studies of the folded conformation. Moreover, the denatured state of a nucleic acid is difficult to study since, like proteins, it is comprised of a large ensemble of conformations. For example, consideration of the number of thermodynamically significant conformations available to each of the seven torsion angles in a dinucleoside monophosphate results in a total of 864 different conformations (*83*, *84*). Winnowing these states down to a single folded state corresponds to a conformational entropy ($\Delta S°$)

loss of −13 cal K^{-1} mol^{-1} (= $-R$ ln 864), which is in reasonable agreement with activation entropy values from rapid kinetic studies on dinucleotide phosphates and polymers (*76*). Moreover, laser *T*-jump relaxation spectroscopy of base stacking in 9,9′-trimethylbisadenine revealed that the joining of two adenines by a conformationally simplified trimethylene bridge increased the forward rate constant for unimolecular stacking (*85*).

Recent theoretical studies have also provided insight into the denatured state of nucleic acids. On the basis of calculations involving only steric constraints, it was estimated that populations of purine nucleotide glycosidic bond conformations can be organized into 2−4 states (*86*). Thus, constraining the glycosidic bond in the denatured state to one conformation would be expected to stabilize the folded state by $\Delta G^{\circ}_{37} \approx 0.4-0.9$ kcal mol^{-1} (= $-T\Delta S = -RT$ ln 2 to $-RT$ ln 4), consistent with k_1 and K values measured here for the 8 nt hairpins. This example serves to illustrate that folding of simple RNA hairpins is limited by a conformational search from an ensemble of heterogeneous unfolded states.

Preorganization in Unmodified Biological Systems. The findings described here raise the question of whether unusually stable, unmodified RNA hairpins derive some of their stability from a preorganized denatured state. The kinetic origin of enhanced stability for the CG closing base pair was demonstrated by gcUUCGgc folding 5.2-fold faster and unfolding 2.3-fold slower than ggUUCGcc at 37.5 °C. These findings provide a role for the CG closing base pair in facilitating both faster folding and slower unfolding. Similar trends are found for rate constant comparisons between 8BrG-substituted gcUUC***G***gc and ggUUC***G***cc. The folding rate constant enhancement might be due to a conformational search accelerated by residual structure in the fully denatured state; however, this would seem unlikely given that a CG closing base pair makes special contributions to stability for diverse tetraloops [e.g., YNMG, GNRA, UUA, and d(GNA)]. Alternatively, enhancement of folding could be driven by favorable electrostatic interactions in nativelike intermediates along the folding pathway. Preliminary nonlinear Poisson−Boltzmann calculations suggest a favorable electrostatic interaction between the loop and a CG, but not a GC, closing base pair (Proctor, D. J. Ph.D. Thesis, The Pennsylvania State University, 2004). It is conceivable that favorable electrostatic interactions stemming from the presence of a CG closing base pair accelerate the conformational search for the native state by guiding stacking arrangements from partially folded states.

ACKNOWLEDGMENT

We are grateful to Dr. Osman Bilsel and the laboratory of Prof. C. R. Matthews for providing us with the nonlinear least-squares program Savuka 5.2.7.

SUPPORTING INFORMATION AVAILABLE

UV and NMR thermal denaturation data for unmodified and 8BrG-substituted gcUUCGgc and ggUUCGcc and a relaxation trace at $T \gg T_M$ for ggUUCGcc (PDF). This information is available free of charge via the Internet at http://pubs.acs.org.

REFERENCES

1. Turner, D. H., Sugimoto, N., and Freier, S. M. (1990) Thermodynamics and kinetics of base-pairing and of DNA and RNA self-assembly and helix coil transition, *Nucleic Acids*, Landolt-Bornstein Series Vol. 1C, pp 201−227, Springer Verlag.: Berlin.
2. Bina-Stein, M., and Stein, A. (1976) Allosteric interpretation of Mg2+ binding to the denaturable Escherichia coli tRNAGlu2+, *Biochemistry 15*, 3912−3917.
3. Brion, P., and Westhof, E. (1997) Hierarchy and dynamics of RNA folding, *Annu. Rev. Biophys. Biomol. Struct. 26*, 113−137.
4. Rook, M. S., Treiber, D. K., and Williamson, J. R. (1999) An optimal Mg(2+) concentration for kinetic folding of the tetrahymena ribozyme, *Proc. Natl. Acad. Sci. U.S.A. 96*, 12471−12476.
5. Tinoco, I., Jr., and Bustamante, C. (1999) How RNA folds, *J. Mol. Biol. 293*, 271−281.
6. Treiber, D. K., and Williamson, J. R. (2001) Beyond kinetic traps in RNA folding, *Curr. Opin. Struct. Biol. 11*, 309−314.
7. Lu, M., and Draper, D. E. (1994) Bases defining an ammonium and magnesium ion-dependent tertiary structure within the large subunit ribosomal RNA, *J. Mol. Biol. 244*, 572−585.
8. Thirumalai, D. (1998) Native secondary structure formation in RNA may be a slave to tertiary folding, *Proc. Natl. Acad. Sci. U.S.A. 95*, 11506−11508.
9. Wu, M., and Tinoco, I., Jr. (1998) RNA folding causes secondary structure rearrangement, *Proc. Natl. Acad. Sci. U.S.A. 95*, 11555−11560.
10. Silverman, S. K., Zheng, M., Wu, M., Tinoco, I., Jr., and Cech, T. R. (1999) Quantifying the energetic interplay of RNA tertiary and secondary structure interactions, *RNA 5*, 1665−1674.
11. Pan, T., Artsimovitch, I., Fang, X. W., Landick, R., and Sosnick, T. R. (1999) Folding of a large ribozyme during transcription and the effect of the elongation factor NusA, *Proc. Natl. Acad. Sci. U.S.A. 96*, 9545−9550.
12. Diegelman-Parente, A., and Bevilacqua, P. C. (2002) A mechanistic framework for co-transcriptional folding of the HDV genomic ribozyme in the presence of downstream sequence, *J. Mol. Biol. 324*, 1−16.
13. Heilman-Miller, S. L., and Woodson, S. A. (2003) Effect of transcription on folding of the Tetrahymena ribozyme, *RNA 9*, 722−733.
14. Ansari, A., Kuznetsov, S. V., and Shen, Y. (2001) Configurational diffusion down a folding funnel describes the dynamics of DNA hairpins, *Proc. Natl. Acad. Sci. U.S.A. 98*, 7771−7776.
15. Fang, X. W., Golden, B. L., Littrell, K., Shelton, V., Thiyagarajan, P., Pan, T., and Sosnick, T. R. (2001) The thermodynamic origin of the stability of a thermophilic ribozyme, *Proc. Natl. Acad. Sci. U.S.A. 98*, 4355−4360.
16. Wallace, M. I., Ying, L., Balasubramanian, S., and Klenerman, D. (2001) Non-Arrhenius kinetics for the loop closure of a DNA hairpin, *Proc. Natl. Acad. Sci. U.S.A. 98*, 5584−5589.
17. Sosnick, T. R., and Pan, T. (2002) Getting hotter with RNA, *Nat. Struct. Biol. 9*, 795−796.
18. Zhang, W., and Chen, S. J. (2002) RNA hairpin-folding kinetics, *Proc. Natl. Acad. Sci. U.S.A. 99*, 1931−1936.
19. Fang, X. W., Srividya, N., Golden, B. L., Sosnick, T. R., and Pan, T. (2003) Stepwise conversion of a mesophilic to a thermophilic ribozyme, *J. Mol. Biol. 330*, 177−183.
20. Cheong, C., Varani, G., and Tinoco, I., Jr. (1990) Solution structure of an unusually stable RNA hairpin, 5′GGAC(UUCG)GUCC, *Nature 346*, 680−682.
21. Varani, G., Cheong, C., and Tinoco, I., Jr. (1991) Structure of an unusually stable RNA hairpin, *Biochemistry 30*, 3280−3289.
22. Williams, D. J., and Hall, K. B. (2000) Experimental and theoretical studies of the effects of deoxyribose substitutions on the stability of the UUCG tetraloop, *J. Mol. Biol. 297*, 251−265.
23. Williams, D. J., Boots, J. L., and Hall, K. B. (2001) Thermodynamics of 2′-ribose substitutions in UUCG tetraloops, *RNA 7*, 44−53.
24. Proctor, D. J., Schaak, J. E., Bevilacqua, J. M., Falzone, C. J., and Bevilacqua, P. C. (2002) Isolation and characterization of a family of stable RNA tetraloops with the motif YNMG that participate in tertiary interactions, *Biochemistry 41*, 12062−12075.
25. Du, Z., Yu, J., Andino, R., and James, T. L. (2003) Extending the family of UNCG-like tetraloop motifs: NMR structure of a CACG tetraloop from coxsackievirus B3, *Biochemistry 42*, 4373−4383.

26. Finger, L. D., Trantirek, L., Johansson, C., and Feigon, J. (2003) Solution structures of stem-loop RNAs that bind to the two N-terminal RNA-binding domains of nucleolin, *Nucleic Acids Res. 31*, 6461−6472.
27. Theimer, C. A., Finger, L. D., and Feigon, J. (2003) YNMG tetraloop formation by a dyskeratosis congenita mutation in human telomerase RNA, *RNA 9*, 1446−1455.
28. Sarma, R. H., Lee, C. H., Evans, F. E., Yathindra, N., and Sundaralingam, M. (1974) Probing the interrelation between the glycosyl torsion, sugar pucker, and the backbone conformation in C(8) substituted adenine nucleotides by 1H and 1H−(31P) fast Fourier transform nuclear magnetic resonance methods and conformational energy calculations, *J. Am. Chem. Soc. 96*, 7337−7348.
29. Proctor, D. J., Kierzek, E., Kierzek, R., and Bevilacqua, P. C. (2003) Restricting the conformational heterogeneity of RNA by specific incorporation of 8-bromoguanosine, *J. Am. Chem. Soc. 125*, 2390−2391.
30. Michelson, A. M., Monny, C., and Kapuler, A. M. (1970) Poly 8-bromoguanylic acid, *Biochim. Biophys. Acta 217*, 7−17.
31. Tavale, S. S., and Sobell, H. M. (1970) Crystal and molecular structure of 8-bromoguanosine and 8-bromoadenosine, two purine nucleosides in the syn conformation, *J. Mol. Biol. 48*, 109−123.
32. Ikehara, M., Uesugi, S., and Yoshida, K. (1972) Studies on the conformation of purine nucleosides and their 5′-phosphates, *Biochemistry 11*, 830−836.
33. Dias, E., Battiste, J. L., and Williamson, J. R. (1994) Chemical probe for glycosidic conformation in telomeric DNAs, *J. Am. Chem. Soc. 116*, 4479−4480.
34. Williams, D. J., and Hall, K. B. (2000) Experimental and computational studies of the G[UUCG]C RNA tetraloop, *J. Mol. Biol. 297*, 1045−1061.
35. Xia, T., SantaLucia, J., Jr., Burkard, M. E., Kierzek, R., Schroeder, S. J., Jiao, X., Cox, C., and Turner, D. H. (1998) Thermodynamic parameters for an expanded nearest-neighbor model for formation of RNA duplexes with Watson−Crick base pairs, *Biochemistry 37*, 14719−14735.
36. Antao, V. P., Lai, S. Y., and Tinoco, I., Jr. (1991) A thermodynamic study of unusually stable RNA and DNA hairpins, *Nucleic Acids Res. 19*, 5901−5905.
37. Antao, V. P., and Tinoco, I., Jr. (1992) Thermodynamic parameters for loop formation in RNA and DNA hairpin tetraloops, *Nucleic Acids Res. 20*, 819−824.
38. Borer, P. N. (1975) in *Handbook of Biochemistry and Molecular Biology: Nucleic Acids* (Fasman, G. D., Ed.) pp 597, CRC Press, Cleveland, OH.
39. Richards, E. G. (1975) in *Handbook of Biochemistry and Molecular Biology: Nucleic Acids* (Fasman, G. D., Ed.) pp 597, CRC Press, Cleveland, OH.
40. Zitzewitz, J. A., Bilsel, O., Luo, J., Jones, B. E., and Matthews, C. R. (1995) Probing the Folding Mechanism of a Leucine Zipper Peptide by Stopped-Flow Circular Dichroism Spectroscopy, *Biochemistry 34*, 12812−12819.
41. Bilsel, O., Zitzewitz, J. A., Bowers, K. E., and Matthews, C. R. (1999) Folding mechanism of the alpha-subunit of tryptophan synthase, an alpha/ beta barrel protein: global analysis highlights the interconversion of multiple native, intermediate, and unfolded forms through parallel channels, *Biochemistry 38*, 1018−1029.
42. Puglisi, J. D., and Tinoco, I., Jr. (1989) Absorbance melting curves of RNA, *Methods Enzymol. 180*, 304−325.
43. McDowell, J. A., and Turner, D. H. (1996) Investigation of the structural basis for thermodynamic stabilities of tandem GU mismatches: solution structure of (rGAGGUCUC)2 by two-dimensional NMR and simulated annealing, *Biochemistry 35*, 14077−14089.
44. Bevington, P. R. (1969) *Data Reduction and Error Analysis for the Physical Sciences*, McGraw-Hill, New York.
45. Puglisi, J. D., and Wyatt, J. R. (1995) Biochemical and NMR studies of RNA conformation with an emphasis on RNA pseudoknots, *Methods Enzymol. 261*, 323−350.
46. Shaka, A. J., Keeler, J., and Freeman, R. (1983) Evaluation of a new broadband decoupling sequence: WALTZ-16, *J. Magn. Reson. 53*, 313−340.
47. Cavanagh, J. F., W. J.; Palmer, A. G., III; Skelton, N. J. (1996) *Protein NMR spectroscopy: principles and practice*, Academic Press, New York.
48. Turner, D. H. F., G. W.; Sutin, N.; Beitz, J. V. (1972) Laser Raman temperature-jump study of the kinetics of the triiodide equilibrium. Relaxation times in the 10-8−10-7 second range, *J. Am. Chem. Soc. 94*, 1554.
49. Turner, D. H. (1986) in *Investigations of Rates and Mechanisms of Reactions* (Bernasconi, C. F., Ed.) pp 141−189, John Wiley & Sons: New York.
50. Ballew, R. M. S., J.; Reiner, C.; Gruebele, M. (1996) A single-sweep, nanosecond time resolution laser temperature-jump apparatus, *Rev. Sci. Instrum. 67*, 3694−3699.
51. Gruebele, M. (1999) The Fast Protein Folding Problem, *Annu. Rev. Phys. Chem. 50*, 485−516.
52. Porschke, D. (1974) Model calculations on the kinetics of oligonucleotide double helix coil transitions. Evidence for a fast chain sliding reaction, *Biophys. Chem. 2*, 83−96.
53. Williams, A. P., Longfellow, C. E., Freier, S. M., Kierzek, R., and Turner, D. H. (1989) Laser Temperature-Jump, Spectroscopic, and Thermodynamic Study of Salt Effects on Duplex Formation by dGCATGC, *Biochemistry 28*, 4283−4291.
54. LeCuyer, K. A., and Crothers, D. M. (1994) Kinetics of an RNA conformational switch, *Proc. Natl. Acad. Sci. U.S.A. 91*, 3373−3377.
55. Menger, M., Eckstein, F., and Porschke, D. (2000) Dynamics of the RNA hairpin GNRA tetraloop, *Biochemistry 39*, 4500−4507.
56. Shen, Y. K., S. V.; Ansari, A. (2001) Loop Dependence of the Dynamics of DNA Hairpins, *J. Phys. Chem. B 105*, 12202−12211.
57. Gruebele, M. S., J.; Ballew, R.; Ervin, J. (1998) Laser Temperature Jump Induced Protein Refolding, *Acc. Chem. Res. 31*, 699−707.
58. Sabelko, J., Ervin, J., and Gruebele, M. (1999) Observation of strange kinetics in protein folding, *Proc. Natl. Acad. Sci. U.S.A. 96*, 6031−6036.
59. Ervin, J., Sabelko, J., and Gruebele, M. (2000) Submicrosecond real-time fluorescence sampling: application to protein folding, *J. Photochem. Photobiol., B 54*, 1−15.
60. Yamamoto, K. M., Y.; Kitagawa, T. (2000) Construction of Novel Nanosecond Temperature Jump Apparatuses Applicable to Raman Measurements and Direct Observation of Transient Temperature, *Appl. Spectrosc. 54*, 1591−1604.
61. Yamamoto, K., Mizutani, Y., and Kitagawa, T. (2000) Nanosecond temperature jump and time-resolved Raman study of thermal unfolding of ribonuclease A, *Biophys. J. 79*, 485−495.
62. Snow, C. D., Nguyen, H., Pande, V. S., and Gruebele, M. (2002) Absolute comparison of simulated and experimental protein-folding dynamics, *Nature 420*, 102−106.
63. Tinoco, I., Jr., and Schmitz, M. (2000) in *Thermodynamics in Biology* (Di Cera, E., Ed.) pp 144−145, Oxford University Press, New York.
64. Bernasconi, C. F. (1976) *Relaxation Kinetics*, Academic Press, New York.
65. Yang, W. Y., and Gruebele, M. (2003) Folding at the speed limit, *Nature 423*, 193−197.
66. Molinaro, M., and Tinoco, I., Jr. (1995) Use of ultra stable UNCG tetraloop hairpins to fold RNA structures: thermodynamic and spectroscopic applications, *Nucleic Acids Res. 23*, 3056−3063.
67. Abdelkafi, M. L., N.; Ghomi, M.; Hervé du Penhoat, C.; Namane, A.; Gouyette, C.; Huynh-Dinh, T.; Baumruk, V.; Turpin, P.-Y. (1997) UNCG tetraloops in short oligoribonucleotides reveal high thermodynamic stability and unusual structural properties in aqueous phase as confirmed by optical and NMR spectroscopies, *J. Mol. Struct. 408/409*, 241−245.
68. Abdelkafi, M., Ghomi, M., Turpin, P. Y., Baumruk, V., Herve du Penhoat, C., Lampire, O., Bouchemal-Chibani, N., Goyer, P., Namane, A., Gouyette, C., Huynh-Dinh, T., and Bednarova, L. (1997) Common structural features of UUCG and UACG tetraloops in very short hairpins determined by UV absorption, Raman, IR and NMR spectroscopies, *J. Biomol. Struct. Dyn. 14*, 579−593.
69. Abdelkafi, M., Leulliot, N., Baumruk, V., Bednarova, L., Turpin, P. Y., Namane, A., Gouyette, C., Huynh-Dinh, T., and Ghomi, M. (1998) Structural features of the UCCG and UGCG tetraloops in very short hairpins as evidenced by optical spectroscopy, *Biochemistry 37*, 7878−7884.
70. Mathews, D. H., Sabina, J., Zuker, M., and Turner, D. H. (1999) Expanded sequence dependence of thermodynamic parameters improves prediction of RNA secondary structure, *J. Mol. Biol. 288*, 911−940.
71. Zuker, M. (2003) Mfold web server for nucleic acid folding and hybridization prediction, *Nucleic Acids Res. 31*, 3406−3415.

72. Sorin, E. J., Engelhardt, M. A., Herschlag, D., and Pande, V. S. (2002) RNA simulations: probing hairpin unfolding and the dynamics of a GNRA tetraloop, *J. Mol. Biol. 317*, 493−506.
73. Sorin, E. J., Rhee, Y. M., Nakatani, B. J., and Pande, V. S. (2003) Insights into nucleic acid conformational dynamics from massively parallel stochastic simulations, *Biophys. J. 85*, 790−803.
74. Tuerk, C., Gauss, P., Thermes, C., Groebe, D. R., Gayle, M., Guild, N., Stormo, G., d'Aubenton-Carafa, Y., Uhlenbeck, O. C., Tinoco, I., Jr., and et al. (1988) CUUCGG hairpins: extraordinarily stable RNA secondary structures associated with various biochemical processes, *Proc. Natl. Acad. Sci. U.S.A. 85*, 1364−1368.
75. Persson, T., Hartmann, R. K., and Eckstein, F. (2002) Selection of hammerhead ribozyme variants with low Mg2+ requirement: importance of stem-loop II, *ChemBioChem 3*, 1066−1071.
76. Turner, D. H. (2000) in *Nucleic Acids: Structures, Properties, and Functions* (Bloomfield, V. A., Crothers, D. M., and Tinoco, I., Jr., Eds.) pp 259−334, University Science Books, Sausalito, CA.
77. Shortle, D., and Ackerman, M. S. (2001) Persistence of native-like topology in a denatured protein in 8 M urea, *Science 293*, 487−489.
78. Srinivasan, R., and Rose, G. D. (1999) A physical basis for protein secondary structure, *Proc. Natl. Acad. Sci. U.S.A. 96*, 14258−14263.
79. Baldwin, R. L., and Zimm, B. H. (2000) Are denatured proteins ever random coils? *Proc. Natl. Acad. Sci. U.S.A. 97*, 12391−12392.
80. Srinivasan, R., and Rose, G. D. (2002) Methinks it is like a folding curve, *Biophys. Chem. 101*−*102*, 167−171.
81. Levinthal, C. (1969) in *Mössbauer Spectroscopy in Biological Systems* (Debrunner, P., Tsibris, J. C. M., and Münck, E., Eds.) pp 22−24, University of Illinois Press, Urbana, IL.
82. Arnold, U., Hinderaker, M. P., Koditz, J., Golbik, R., Ulbrich-Hofmann, R., and Raines, R. T. (2003) Protein prosthesis: a nonnatural residue accelerates folding and increases stability, *J. Am. Chem. Soc. 125*, 7500−7501.
83. Berman, H. M. (1981) in *Topics in Nucleic Acid Structure* (Neidle, S., Ed.), Macmillan, London, U.K.
84. Olson, W. K. (1982) in *Topics in Nucleic Acid Structure* (Neidle, S., Ed.), Macmillan, London, U.K.
85. Pörschke, D. (1978) Molecular States in Single-Stranded Adenylate Chains by Relaxation Analysis, *Biopolymers 17*, 315−323.
86. Murthy, V. L., Srinivasan, R., Draper, D. E., and Rose, G. D. (1999) A complete conformational map for RNA, *J. Mol. Biol. 291*, 313−327.
87. Wimberly, B. T., Brodersen, D. E., Clemons, W. M., Jr., Morgan-Warren, R. J., Carter, A. P., Vonrhein, C., Hartsch, T., and Ramakrishnan, V. (2000) Structure of the 30S ribosomal subunit, *Nature 407*, 327−339.
88. Cannone, J. J., Subramanian, S., Schnare, M. N., Collett, J. R., D′Souza, L. M., Du, Y., Feng, B., Lin, N., Madabusi, L. V., Muller, K. M., Pande, N., Shang, Z., Yu, N., and Gutell, R. R. (2002) The Comparative RNA Web (CRW) Site: an online database of comparative sequence and structure information for ribosomal, intron, and other RNAs, *BMC Bioinf. 3*, 2.

BI048213E